Reynolds Number Effects on the Non-Nulling Calibration of a Cone-Type Five-Hole Probe for Turbomachinery Applications

Sang Woo Lee*, Sang Bae Jun

*School of Mechanical Engineering, Kumoh National Institute of Technology,
188 Shinpyong, Gumi, Gyongbook 730-701, Republic of Korea*

The effects of Reynolds number on the non-nulling calibration of a typical cone-type five-hole probe have been investigated for the representative Reynolds numbers in turbomachinery. The pitch and yaw angles are changed from -35 degrees to 35 degrees with an angle interval of 5 degrees at six probe Reynolds numbers in range between 6.60×10^3 and 3.17×10^4. The result shows that not only each calibration coefficient itself but also its Reynolds number dependency is affected significantly by the pitch and yaw angles. The Reynolds-number effects on the pitch- and yaw-angle coefficients are noticeable when the absolute values of the pitch and yaw angles are smaller than 20 degrees. The static-pressure coefficient is sensitive to the Reynolds number nearly all over the pitch- and yaw-angle range. The Reynolds-number effect on the total-pressure coefficient is found remarkable when the absolute values of the pitch and yaw angles are larger than 20 degrees. Through a typical non-nulling reduction procedure, actual reduced values of the pitch and yaw angles, static and total pressures, and velocity magnitude at each Reynolds number are obtained by employing the calibration coefficients at the highest Reynolds number ($\text{Re}=3.17 \times 10^4$) as input reference calibration data. As a result, it is found that each reduced value has its own unique trend depending on the pitch and yaw angles. Its general tendency is related closely to the variation of the corresponding calibration coefficient with the Reynolds number. Among the reduced values, the reduced total pressure suffers the most considerable deviation from the measured one and its dependency upon the pitch and yaw angles is most noticeable. In this study, the root-mean-square data as well as the upper and lower bounds of the reduced values are reported as a function of the Reynolds number. These data would be very useful in the estimation of the Reynolds-number effects on the non-nulling calibration.

Key Words : Five-Hole Probe, Non-Nulling Calibration, Reynolds Number, Turbomachinery

Nomenclature

C_M : Pseudo Mach number, Eq. (7)
C_{pa} : Pitch-angle coefficient, Eq. (1)
C_{sp} : Static-pressure coefficient, Eq. (3)
C_{tp} : Total-pressure coefficient, Eq. (4)
C_{ya} : Yaw-angle coefficient, Eq. (2)

* Corresponding Author,
  E-mail : swlee@kumoh.ac.kr
  TEL : +82-54-467-4209; FAX : +82-54-467-4050
  School of Mechanical Engineering, Kumoh National
  Institute of Technology, 188 Shinpyong, Gumi, Gyong-
  book 730-701, Republic of Korea. (Manuscript Receiv-
  ed October 10, 2003; Revised Jane 16, 2005)

D : Diameter of five-hole probe
M : Mach number
P_{av} : Average pressure, Eq. (5)
P_i : Pressure measured at the i-th pressure-sensing hole of five-hole probe
P_s : Static pressure or measured static pressure
$P_{s,red}$: Reduced static pressure
P_t : Total pressure or measured total pressure
$P_{t,red}$: Reduced total pressure
Q : Velocity magnitude or measured velocity magnitude
Q_{red} : Reduced velocity magnitude, Eq. (6)
Re_D : Reynolds number $= U_\infty D / \nu$

U_∞ : Free-stream velocity

Greek symbols

α : Pitch angle or rotated pitch angle
α_{red} : Reduced pitch angle
β : Yaw angle or rotated yaw angle
β_{red} : Reduced yaw angle
ν : Kinematic viscosity

1. Introduction

A five-hole probe is one of the most widely used probes in the measurement of complex three-dimensional flows encountered in various fluid engineering branches (Lee et al., 1994 ; Lee et al., 1997 ; Lee et al., 2001a ; Lee et al., 2001b). Particularly, the five-hole probe is a very useful means for the research and development in turbomachinery, because it directly provides static and total pressures as well as flow angles. It is customary that calibration of the five-hole probe is usually performed at a representative Reynolds number, Re_D, which is based on its head diameter and a reference velocity. The reference velocity may be a free-stream velocity for an external flow or a mean velocity averaged over the cross-section for an internal flow. Since local velocity magnitude at each measurement location is generally different from the reference one, an error arising from the difference between the local and calibration Reynolds numbers cannot be avoidable. This is referred to as a Reynolds-number effect.

Treaster and Yocum (1979) reported a non-nulling calibration technique, typical calibration data and interpolation procedure of five-hole probes of both the angle-tube and prismatic probe heads. They documented variations of the calibration data depending on wall proximity effects as well as the Reynolds number. Hoffman et al.(1980) developed a unified inviscid theoretical model for a five-hole probe with a cone angle of 30 degrees. However, they did not consider the Reynolds-number effect, even though their Reynolds number lies in the most Reynolds-number sensitive range. Sitaram et al. (1981) reported measurement data within the

blade passages of an axial-flow compressor and an axial-flow inducer with conventional pressure probes including a hemispherical five-hole probe. They discussed not only various error sources in the measurements but also a method of estimating these errors. Dominy and Hudson (1993) studied effects of the Reynolds number, Mach number and turbulence on the calibrations of commonly used cone-type and pyramid-head five-hole probes for the Reynolds numbers in range between 7×10^3 and 8×10^4. They found the existence of two distinct Reynolds-number effects. One of them is a flow separation around the probe head at relatively low Reynolds numbers when the probe is at incidence. The other is related to changes in the detailed structure of the flow around the sensing holes even when the probe is nulled. In their study, however, only the yaw angle, β, was changed from -20 degrees to 20 degrees at a fixed pitch angle of $\alpha=0$ degree. Therefore, they could not report the combined effect of the pitch and yaw angles in the whole non-nulling calibration range. In the investigation of the Reynolds-number effects on the non-nulling calibration, actual errors in the pitch and yaw angles, static and total pressures, and velocity magnitude with the variation of the Reynolds number may be of practical importance. Unfortunately, however, there seems to be no available data on them, although the Reynolds-number effects only on the calibration coefficients are reported in part by several investigators such as Treaster and Yocum (1979), Smith and Adcock (1986), and Dominy and Hudson (1993). Recently, Coldrick et al.(2002) provided some considerations for using three-dimensional probes in high-speed multi-stage axial compressors. They focused on the feasibility of employing four-hole probes in an actual compressor environment.

Since a nulling method requires an additional probe-rotating mechanism during flow measurements, the non-nulling calibration is preferred in spite of complexities in its calibration and reduction procedures as well as relatively large measurement errors. However, it is very hard to find open literature which provided the Reynolds-number effects on the calibration coeffi-

cients in the entire pitch- and yaw-angle range. Moreover, there seem to be no systematic investigations that contain the Reynolds-number effects on the reduced flow angles, pressures and velocity magnitude obtained through the non-nulling reduction procedure. In this study, the effects of the Reynolds number on the non-nulling calibration of a typical cone-type five-hole probe have been investigated in the full range of the pitch and yaw angles for the Reynolds numbers covering turbomachinery applications.

2. Experiment

2.1 Cone-type five-hole probe

The five-hole probe used in this study is photographed in Fig. 1. It is a commercially available one (United Electronic Controls, DC-187-12-CD) which has a cone-type probe head with a cobra-shaped stem as in Fig. 2. The centerline of the probe stem passes through the center of the pressure-sensing hole #1, so that the probe tip is always positioned at the same location regardless of yaw-angle changes. As shown in Fig. 2, the probe head has two neighboring cone surfaces. The upstream cone has a cone angle of 90.0 degrees and the downstream cone angle is measured to be 28.6 degrees. The holes from #2 to #5 are oriented perpendicular to the downstream cone surface. As defined in Fig. 2, the

pitch and yaw angles are positive when $P_4 > P_5$ and $P_2 > P_3$, respectively. The five-hole probe has a probe head diameter, D, of 4.75 mm (0.187 inch). Other measured dimensions are presented on the right side in Fig. 2.

2.2 Experimental apparatus

The experimental rig is made up of a small axi-symmetric wind tunnel, a precision two-axis probe rotator, a two-dimensional automatic traverse system, and a data acquisition and control system, as shown in Fig. 2. The wind tunnel is an open-circuit type, and its exit diameter is 50 mm. An 11-kW centrifugal compressor is installed in the wind tunnel, and its exit velocity can be widely varied with an inverter. The precision probe rotator employs an AC servo motor
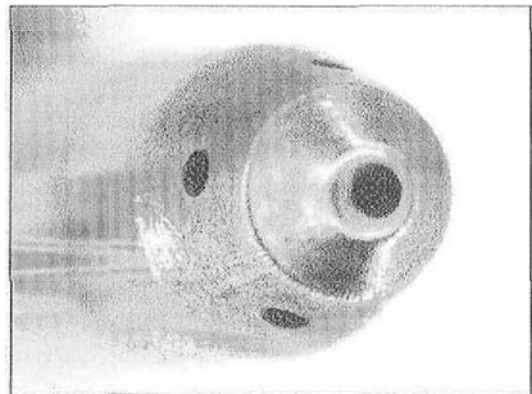

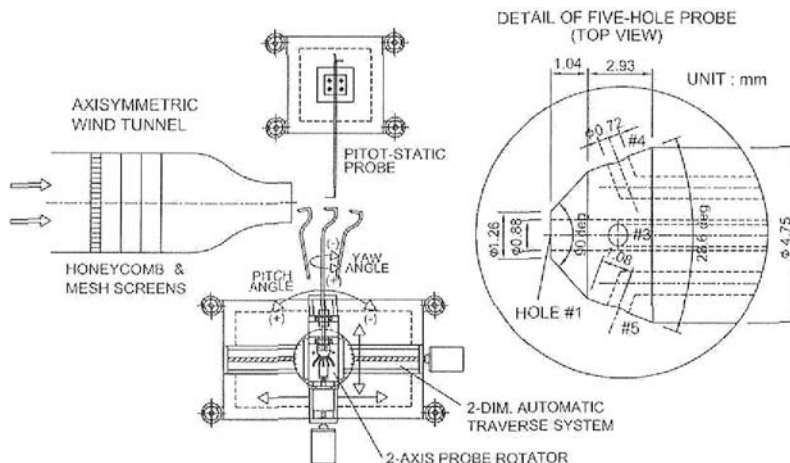Fig. 1   Present cone-type five-hole probe

Fig. 2   Top view of experimental apparatus

with a harmonic reduction gear (Oriental Motor, KXSM240HG1-BL), so that its resolution is only 0.0072 degrees without backlash. The location of the five-hole probe is carefully adjusted with the two-dimensional automatic traverse system equipped with linear-motion guides, stepping motors and stepping-motor drivers. Therefore, its tip is always positioned at the same location even in the case that the five-hole probe is rotated in the pitch-angle direction.

The pressure measurement system employed in this study is basically the same as that of Lee et al. (2001a). All measurements are controlled by a personal computer (IBM, AT 486) equipped with a Multi-Function DI/O Board (National Instruments, AT-MIO-16D-H-9). The automatic traverse system as well as a pressure scanning box (Furness Controls, FC091-6) for sequential switching of the five pressure-sensing holes is controlled by digital-out pulses from the Multi-Function DI/O Board. Measured pressures are transformed into DC voltages by a high-accuracy differential pressure transducer (MKS, Type 120AD-00010RAB). The electric signals are sampled by a 12-bit A-D converter in the Multi-Function DI/O Board, and transferred into the computer. The whole measurement system is controlled in proper sequence by a standalone C-language program.

2.3 Experimental conditions and uncertainties

The Reynolds numbers commonly encountered in turbomachinery applications are approximately in range between Re=5.0×10^3 and 8.0×10^4. Koschel and Pretzsch (1988) showed that effects of the Reynolds number are negligible in the range from Re=3.7×10^4 to 8.2×10^4 for cone-type five-hole probes. Dominy and Hudson (1993) also confirmed that for 60 and 90 degrees perpendicular cone-type probes, effects of the Reynolds number on the yaw-angle coefficient and dynamic-pressure coefficient are important only when the Reynolds number is lower than about 4.0×10^4. For most practical cases, air flows are considered to be incompressible if the Mach number is lower than about 0.3 (Anderson,

1990). Under this condition, the effects of the Reynolds-number could be isolated from the Mach-number effects. In order to keep calibration free-stream velocities lower than about 0.3 of the speed of sound in the aforementioned Reynolds-number range, we choose the five-hole probe of 4.75 mm in diameter as in Fig. 2, which is about two times larger than a commonly-used one. With this probe, calibrations are performed at six Reynolds numbers of 6.60×10^3, 1.30×10^4, 1.92×10^4, 2.44×10^4, 2.87×10^4 and 3.17×10^4. Among these cases, the Mach number only at Re=3.17×10^4, which is evaluated to be M=0.33, is slightly higher than 0.3. At each Reynolds number, the pitch and yaw angles are changed from -35 degrees to 35 degrees with an angle interval of 5 degrees. Turbulence intensity at the exit of the wind tunnel remains at about 1 percent, independent of the free-stream velocity.

Since the calibrations are carried out in low-turbulence and uniform-velocity conditions, the effects of local turbulence (Dominy and Hudson, 1993) and mean velocity gradient (Ligrani et al., 1989) can easily be removed. The uncertainty intervals presented in this study are evaluated with 95 percent confidence (Abernethy et al., 1985). Uncertainties associated with the probe rotation were given to be ± 0.1 degrees in the pitch and yaw angles. The uncertainty in the pressure measurement is estimated to be ± 0.7 percents of the free-stream dynamic pressure. The uncertainty intervals associated with the pitch-angle coefficient, yaw-angle coefficient, static-pressure coefficient and total-pressure coefficient are evaluated to be ± 0.120, ± 0.095, ± 0.023 and ± 0.043, respectively.

3. Results and discussion

3.1 Calibration coefficients

In general, the calibration coefficients in the non-nulling reduction procedure are defined in the following ways (Treaster and Yocum, 1979).

$$C_{pa} = (P_4 - P_5)/(P_1 - P_{av}) \tag{1}$$

$$C_{ya} = (P_2 - P_3)/(P_1 - P_{av}) \tag{2}$$

$$C_{sp} = (P_{av} - P_s)/(P_1 - P_{av}) \qquad (3)$$

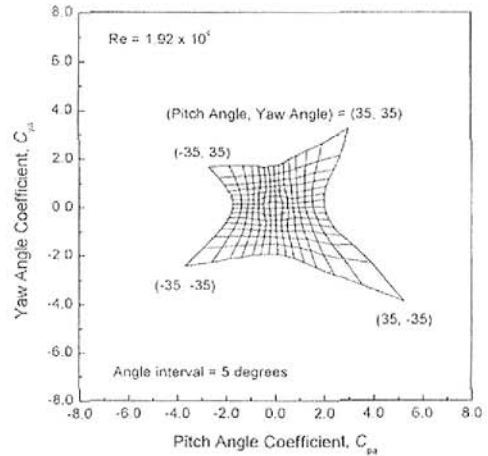$$C_{tp} = (P_1 - P_t)/(P_1 - P_{av}) \qquad (4)$$

Here, C_{pa}, C_{ya}, C_{sp}, and C_{tp} are the pitch-angle coefficient, yaw-angle coefficient, static-pressure coefficient and total-pressure coefficient, respectively. In the above equations, the pressures, P_1, P_2, P_3, P_4 and P_5 are measured at the corresponding pressure-sensing holes and the static pressure, P_s, and the total pressure, P_t, are measured with the pitot-static pressure probe. The pressure, P_{av}, is defined as in Eq. (5).

$$P_{av} = (P_2 + P_3 + P_4 + P_5)/4 \qquad (5)$$

Figure 3 provides typical distributions of the four calibration coefficients in the non-nulling procedure for the present cone-type five-hole probe at Re=1.92×10⁴. It is usual to determine the reduced pitch and yaw angles, α_{red} and β_{red}, from the C_{pa} versus C_{ya} plot in Fig. 3(a), if the values of C_{pa} and C_{ya} at a measurement location are evaluated with measured five pressures as in Eq. (1) and Eq. (2). In this case, it is essential that each pair of C_{pa} and C_{ya} in Fig. 3(a) should be mapped onto just one pair of the pitch and yaw angles all over the calibration range. Once the flow direction has been established from Fig. 3(a), the corresponding values of C_{sp} and C_{tp} can be determined from the contours of C_{sp} (Fig. 3(b)) and of C_{tp} (Fig. 3(c)), and then the reduced static and total pressures, $P_{s,red}$ and $P_{t,red}$, are obtained from Eq. (3) and Eq. (4), respectively. Thus, these subsequent pressure determinations are influenced by the values of α_{red} and β_{red} as well as the contours in Fig. 3(b) and 3(c). Finally, velocity magnitude can be reduced as the following equation.

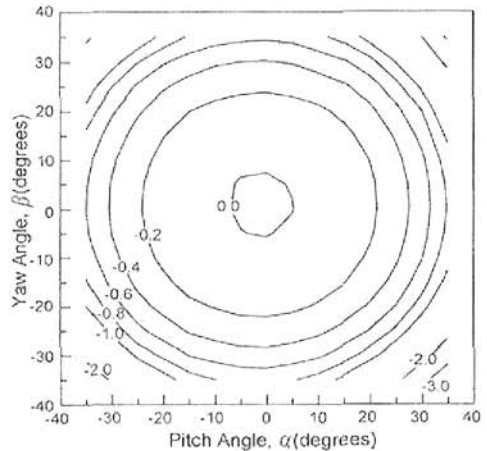$$Q_{red} = \sqrt{\frac{2(P_{t,red} - P_{s,red})}{\rho}} \qquad (6)$$

For compressible flows, a third calibration coefficient, which is related to a third independent variable, Mach number, is required. The pseudo Mach number is defined in the following way (Dominy and Hudson, 1993).

(a) Pitch-angle coefficient versus yaw-angle coefficient
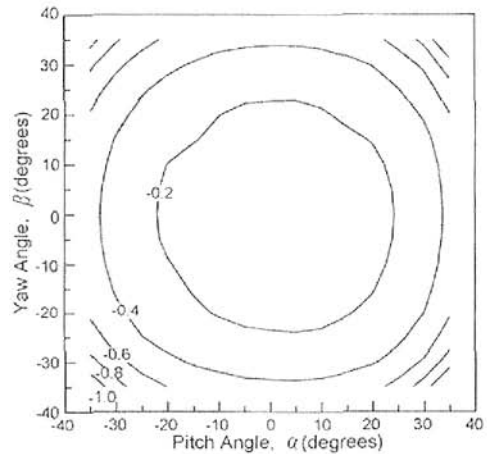
(b) Static-pressure coefficient

(c) Total-pressure coefficient

Fig. 3 Typical Calibration coefficients at Re=1.92×10⁴

$$C_M = P_{av}/P_1 \qquad (7)$$

where C_M is the pseudo Mach Number. The pitch angle, yaw angle and Mach number are determined from the C_{pa}-C_{ya}-C_M relation. Then, the static and total pressures can be obtained from their appropriate coefficients.

3.2 Effects of the Reynolds number on the calibration coefficients

Figure 4 shows the effect of the Reynolds number on the C_{pa} versus C_{ya} plot. In an ideal case, each grid on the C_{pa} versus C_{ya} plot should be a square all over the calibration range. However, this cannot be achieved in a real situation. At

$Re=6.60\times10^3$ (Fig. 4(a)), each grid seems to be nearly rectangular when $|\alpha|$ and $|\beta|<20$ degrees, but is distorted into a diamond shape especially along the diagonal direction when $|\alpha|$ and $|\beta|>20$ degrees. The rectangular calibration grids may result in an accurate determination of the pitch and yaw angles due to a simple interpolation in the reduction procedure, meanwhile a severe distortion from the rectangular shape may deliver greater errors in the flow-angle determination. As the Reynolds number increases, in general, elongation of the grids in the diagonal direction tends to be reduced, and the outermost bound of the grids seems to contract. A direct comparison between the cases at $Re=6.60\times10^3$ (Fig. 4(a))
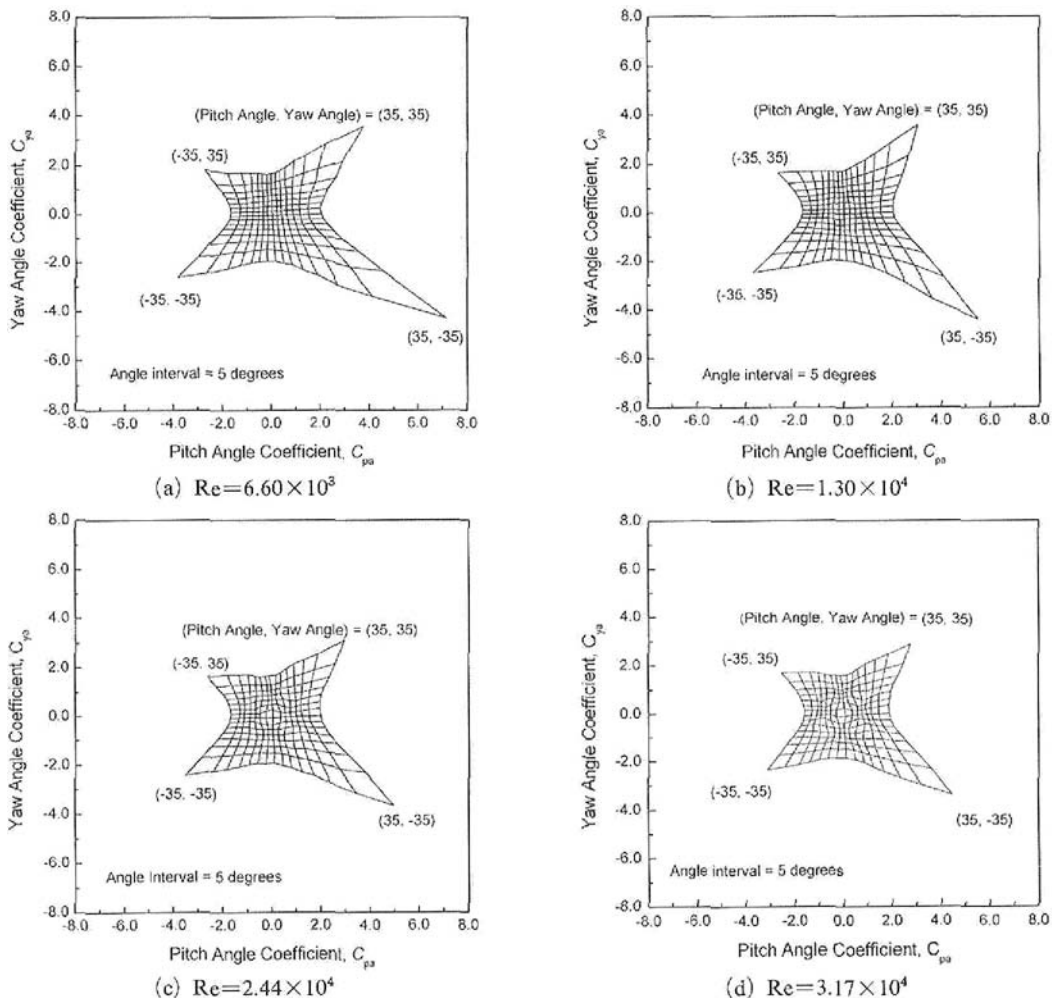

(a) $Re=6.60\times10^3$

(b) $Re=1.30\times10^4$

(c) $Re=2.44\times10^4$

(d) $Re=3.17\times10^4$

Fig. 4 Pitch-angle coefficient versus yaw-angle coefficient

and 3.17×10^4 (Fig. 4(d)) confirms these facts. In addition, it is noted that with increasing the Reynolds number, there is a significant change in the grid shape in the area where $|\alpha|$ and $|\beta| < 20$ degrees. In this area, each rectangular grid is severely deformed into a rather irregular shape. This trend is found to be significant at higher Reynolds numbers as in Fig. 4(c) and (d). The grid points located around the central one of α and $\beta = 0$ degree tend to move away from it, as the Reynolds number increases. These irregular grid shapes may be attributed to the flow change over the two neighboring cone surfaces of the probe head with the variation of the Reynolds number.

Contours of C_{pa} are presented in Fig. 5. In an ideal case, each contour should be a straight vertical line. However, actual contours in Fig. 5 are far from the ideal ones. In general, the contour at around $\alpha = 0$ degree approaches the ideal one, although it is not perfectly vertical. As $|\alpha|$ increases, the contours tend to be curved. This tendency is always found regardless of the Reynolds number. The most noticeable change in C_{pa} at higher Reynolds numbers is a wavy variation in the β-direction in the area of $|\alpha|$ and $|\beta| < 20$ degrees, as in Fig. 5(c) and (d). This change in C_{pa} with the Reynolds number is found most remarkable along the line of $\beta = 0$ degree, when $|\alpha| < 20$ degrees. On the other hand, the
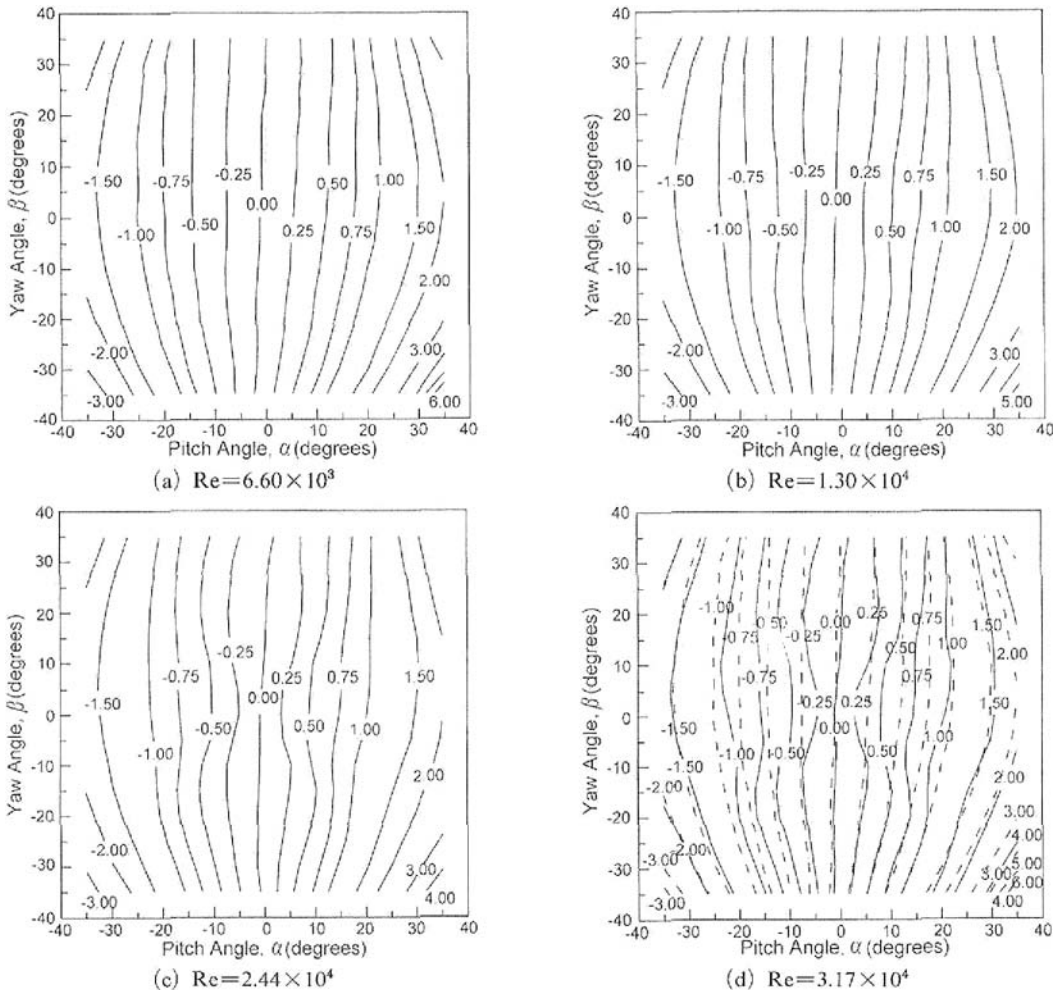

(a) $Re = 6.60 \times 10^3$

(b) $Re = 1.30 \times 10^4$

(c) $Re = 2.44 \times 10^4$

(d) $Re = 3.17 \times 10^4$

Fig. 5 Contours of pitch-angle coefficient, C_{pa}

contour at $\alpha = 0$ degree still remains nearly straight even at $Re = 3.17 \times 10^4$ (Fig. 5(d)). It is noted along the line of $\beta = 0$ degree in Fig. 5(d) that the absolute value of C_{pa} at $Re = 6.60 \times 10^3$ is lower than that at $Re = 3.17 \times 10^4$ in the region of $|\alpha| < 20$ degrees. Contours of C_{ya} presented in Fig. 6 show a similar trend to those of C_{pa}. In an ideal case, contours of C_{ya} should be in the form of a straight horizontal line. Each actual contour in Fig. 6 is different from that in the ideal case, particularly at large $|\beta|$. At higher Reynolds numbers (Fig. 6(c) and (d)), there is a wavy variation of C_{ya} in the α-direction when $|\alpha|$ and $|\beta| < 20$ degrees. Along the line of $\alpha = 0$ degree in Fig. 6(d), the absolute value of C_{ya} at

$Re = 6.60 \times 10^3$ is lower than that at $Re = 3.17 \times 10^4$ when $|\beta| < 20$ degrees. The wavy variations in C_{pa} and C_{ya} are related closely to the irregular grid shapes found in the central regions of Fig. 4 (c) and (d).

Contours of C_{sp} for different Reynolds numbers are shown in Fig. 7. In Fig. 7(a), the value of C_{sp} lies only in a narrow range of $-0.4 < C_{sp} < 0.0$, in most areas except the corners. In the case of $Re = 6.60 \times 10^3$, each contour is not symmetric with respect to the line of $\alpha = 0$ degree. With increasing the Reynolds number, however, each contour approaches a symmetric distribution. This fact means that the effect of the probe stem becomes relatively small in high
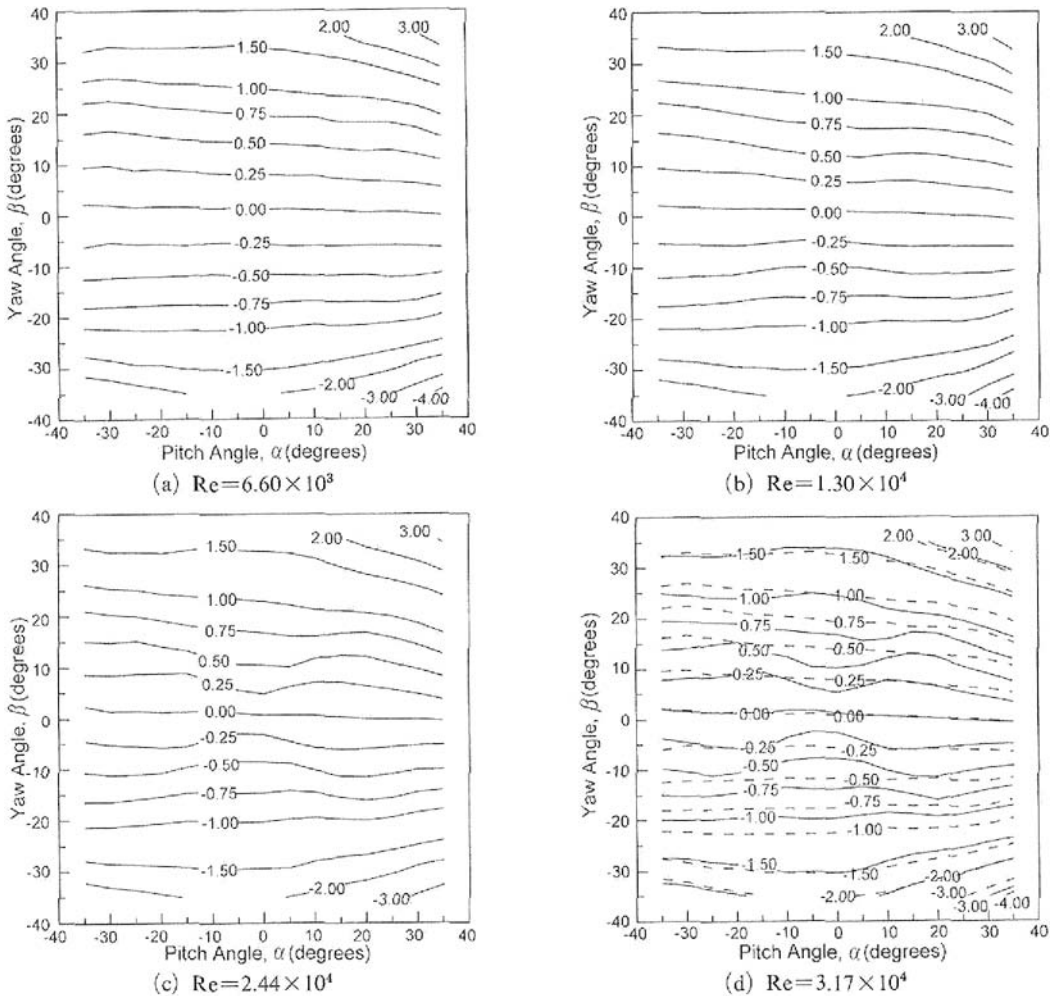

Fig. 6 Contours of yaw-angle coefficient, C_{ya}

Reynolds-number flows. It is particularly interesting that the contour of $C_{sp} = -0.2$ is deformed into a "+" shape when $Re \geq 2.44 \times 10^4$. A close examination of the two types of contours in Fig. 7(d) shows that there is a noticeable Reynolds-number effect on C_{sp} in the entire region except the corner areas. Moreover, C_{sp} at $Re = 6.60 \times 10^3$ always has a higher value than that at $Re = 3.17 \times 10^4$ all over the calibration range. Treaster and Yocum (1979), and Dominy and Hudson (1993) also reported noticeable Reynolds-number effects on C_{sp}.

The effect of the Reynolds number on C_{tp} is introduced in Fig. 8. Independent of the Reynolds number, contours of C_{tp} seem to be nearly concentric. The value of C_{tp} at $Re = 6.60 \times 10^3$ in Fig. 8(a) changes significantly from about -5.0 to about zero. On the other hand, the value of C_{sp} in Fig. 7(a) varies from about -1.0 to about zero. Therefore, the gradient of C_{tp} is much steeper than that of C_{sp}, especially in the corner areas. A direct comparison of C_{tp} between the two cases of $Re = 6.60 \times 10^3$ and 3.17×10^4 in Fig. 8(d) shows that its difference is found to be minute in the region surrounded by the contour of $C_{tp} = -0.4$ excluding the area just around the point of α and $\beta = 0$ degree. At the corners in Fig. 8(d), however, there are remarkable changes in C_{tp} between the two types of contours, especially when $|\alpha|$ and $|\beta| > 20$ degrees. In the entire
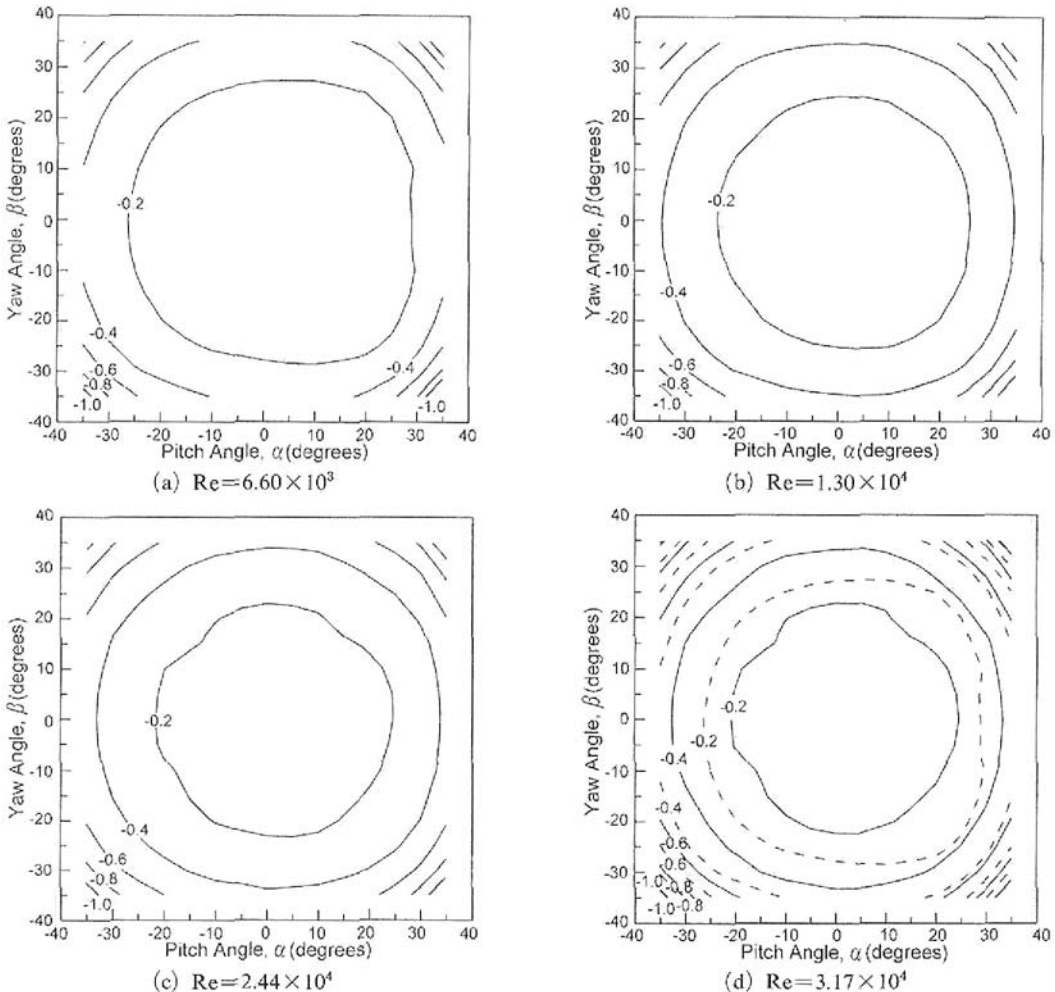

(a) $Re = 6.60 \times 10^3$

(b) $Re = 1.30 \times 10^4$

(c) $Re = 2.44 \times 10^4$

(d) $Re = 3.17 \times 10^4$

Fig. 7   Contours of static-pressure coefficient, C_{sp}

calibration region except the area near the center in Fig. 8(d), C_{tp} at Re=6.60×10³ has a lower value than that at Re=3.17×10³. This is a totally different tendency in comparison with the behavior of C_{sp} in Fig. 7(d). From Figs. 7(d) and 8 (d), the Reynolds-number effect on C_{tp} is found more significant than that on C_{sp}, when $|\alpha|$ and $|\beta|>20$ degrees. On the other hand, C_{sp} is more sensitive to the Reynolds number than C_{tp} in the other calibration range.

The calibration coefficients in this non-nulling mode, in general, do not show concentric distributions with respect to the center point of α and $\beta=0$ degree except for the total-pressure coefficient in Fig. 8. Therefore, previous Reynolds-number dependencies for -20 degrees$\leq\beta\leq20$ degrees at $\alpha=0$ degree by Dominy and Hudson (1993) cannot provide the full calibration characteristics. In summary, the pitch- and yaw-angle coefficients have nearly the same trend with the Reynolds number, and their Reynolds-number dependencies are considerable when $|\alpha|$ and $|\beta|<20$ degrees. The static-pressure coefficient is found sensitive to the Reynolds number nearly all over the pitch- and yaw-angle range. There exists a dominant Reynolds-number effect on the total-pressure coefficient when $|\alpha|$ and $|\beta|>20$ degrees, which seems to be the most noticeable Reynolds-number effect among the four calibration coefficients.
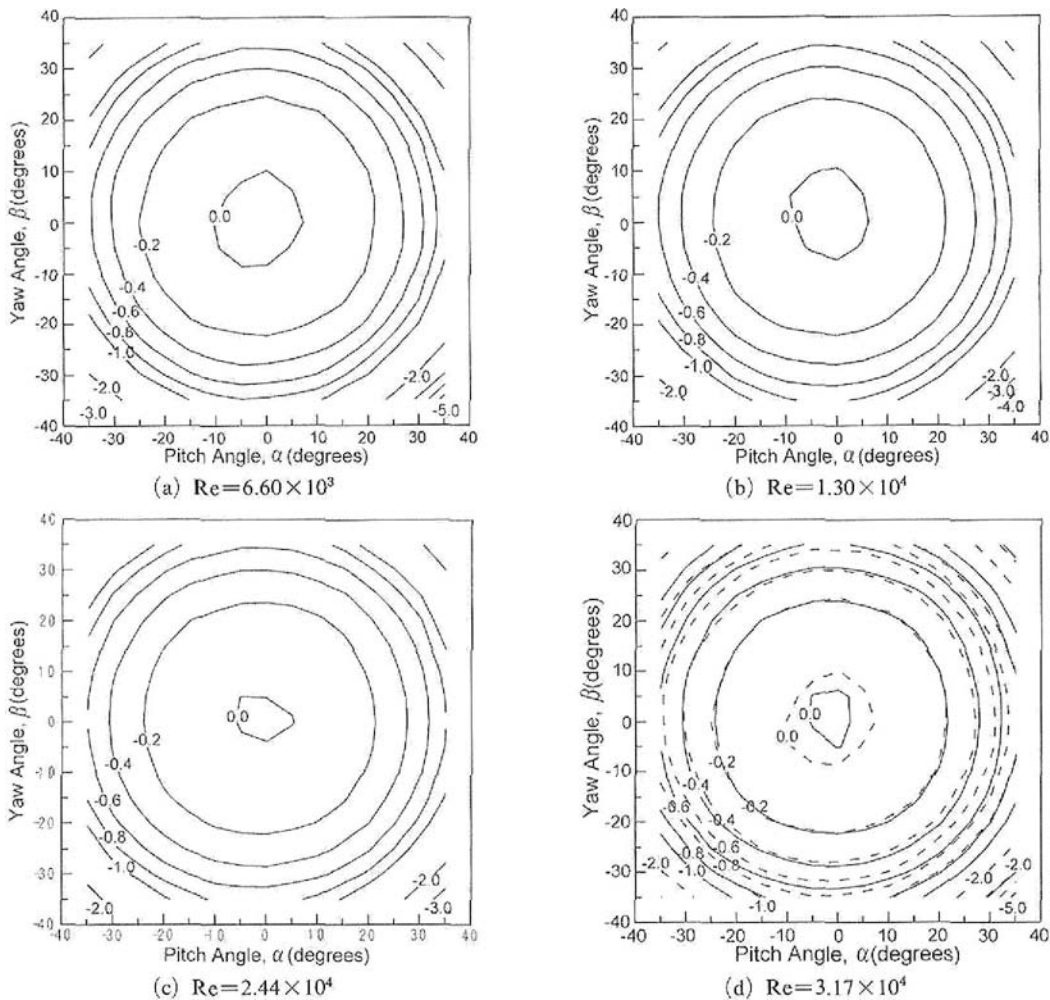

(a) Re=6.60×10³

(b) Re=1.30×10⁴

(c) Re=2.44×10⁴

(d) Re=3.17×10⁴

Fig. 8 *Contours of total-pressure coefficient,* C_{tp}

3.3 Effects of the Reynolds number on the reduced flow angles, pressures and velocity magnitude

In the previous figures (Figs. 4~8), the effects of the Reynolds number on the calibration coefficients are discussed in detail. In addition to these, it would be of practical importance to know the actual amounts of changes in the pitch angle, yaw angle, static pressure, total pressure and velocity magnitude due to the Reynolds-number variation. For this purpose, we employed a non-nulling data reduction program that was developed by Lee et al.(2001a). In this program, cubic spline functions are used for the interpolation of the calibration data (Prenter, 1975). In the investigation of turbomachinery, it is important to understand the flow phenomena near machine surfaces and in the wake regions where most of aerodynamic losses are generated. In these regions, local velocity magnitudes may be lower than the corresponding free-stream velocity. Noting this fact, 169 (13×13) sets of five measured pressures (-30 degrees $\leq \alpha$ and $\beta \leq 30$ degrees) in the cases of Re=6.60×10^3, 1.30×10^4, 1.92×10^4, 2.44×10^4 and 2.87×10^4 are applied to the non-nulling reduction program, employing the calibration coefficients at the highest Reynolds number of Re=3.17×10^4 as input reference calibration data. Then, the reduced 169 sets of the pitch angle, yaw angle, static pressure, total pressure and velocity magnitude at each Reynolds number are compared with the corresponding

measured values. Particularly near the machine surfaces, a wall-proximity effect should be considered in addition to the Reynolds number effect (Lee and Yoon, 1999).

The pitch-angle difference, $(\alpha_{red}-\alpha)$, is given in Fig. 9 in the cases of Re=6.60×10^3 and 1.30×10^4. At Re=6.60×10^3 (Fig. 9(a)), $(\alpha_{red}-\alpha)$ suffers a considerable change with the variation of the pitch and yaw angles. As the pitch angle increases from -30 degrees at relatively small yaw angles such as $\beta=-5$, 0 and 5 degrees, $(\alpha_{red}-\alpha)$ increases and has a maximum value. Then, it decreases to a negative minimum value and show an increasing tendency again. Regardless of the yaw angle, the absolute value of $(\alpha_{red}-\alpha)$ is smallest at $\alpha=0$ degree. These tendencies are related closely to the difference in C_{pa} between the cases of Re=6.60×10^3 and 3.17×10^4 (Fig. 5 (d)). In general, larger discrepancies between the dotted and solid lines in Fig. 5(d) result in greater absolute value of $(\alpha_{red}-\alpha)$. When the value of C_{pa} is higher than that at the reference Reynolds number (Re=3.17×10^4), $(\alpha_{red}-\alpha)$ has a positive value, and vice versa. The upper and lower bounds of $(\alpha_{red}-\alpha)$ all over the pitch and yaw angles are 4.9 and -4.3 degrees, respectively. These values are located at the pitch and yaw angles where there exist the largest discrepancies between the dotted and solid lines in Fig. 5(d). These tendencies of $(\alpha_{red}-\alpha)$ at Re=1.30×10^4 (Fig. 9(b)) are very similar to those at Re=6.60×10^3, but its absolute values tend to
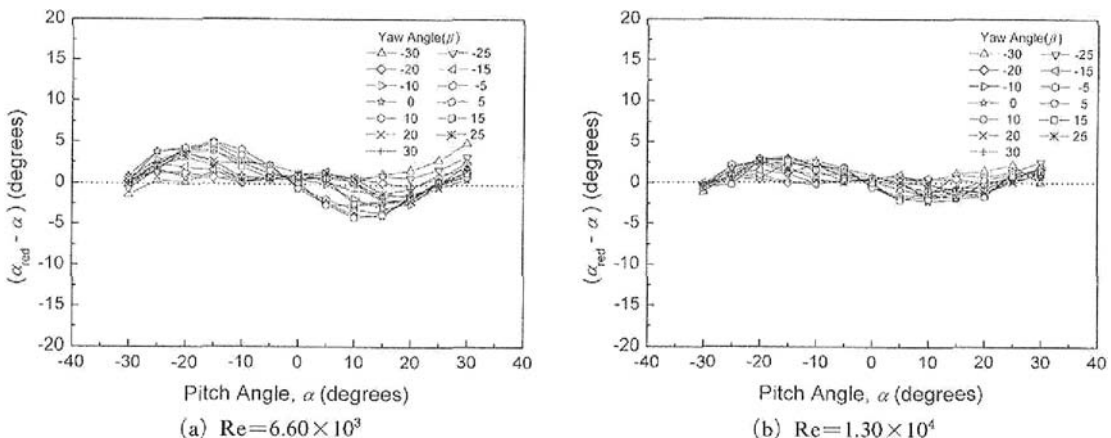

(a) Re=6.60×10^3

(b) Re=1.30×10^4

Fig. 9 $(\alpha_{red}-\alpha)$ obtained with calibration coefficients at Re=3.17×10^4

decrease in comparison with those in Fig. 9(a).

The yaw-angle difference, $(\beta_{red} - \beta)$, is introduced in Fig. 10. At Re=6.60×10³ (Fig. 10 (a)), $(\beta_{red} - \beta)$ also depends strongly on the pitch and yaw angles. As the yaw angle increases from −30 degrees at relatively small pitch angles such as $\alpha = -5$, 0 and 5 degrees, $(\beta_{red} - \beta)$ has nearly the same trend as $(\alpha_{red} - \alpha)$. Independent of the pitch angle, $(\beta_{red} - \beta)$ has relatively small values at $\beta = 0$ degrees. These are resulted mainly from the discrepancies of C_{ya} at Re=6.60×10³ from that at Re=3.17×10⁴ as shown in Fig. 6(d). The upper and lower bounds of $(\beta_{red} - \beta)$ are found to be 4.4 and −4.4 degrees, respectively. When C_{ya} is higher than that at the reference Reynolds number (Re=3.17×10⁴), $(\beta_{red} - \beta)$

has a positive value, and vice versa. At Re≈ 1.30×10⁴ (Fig. 10(b)), the absolute value of $(\beta_{red} - \beta)$ tends to decrease in comparison with that in Fig. 10(a), and falls within about 3.0 degrees. From the results in Figs. 9 and 10, it is confirmed that the general trend of $(\alpha_{red} - \alpha)$ with α is nearly the same as that of $(\beta_{red} - \beta)$ with β.

The reduced static-pressure difference normalized by $\rho U_\infty^2/2$, $(P_{s,red} - P_s)/(\rho U_\infty^2/2)$, is given in Fig. 11. Examining the results in Fig. 7(d), C_{sp} at Re= 6.60×10³ has a higher value than that at the reference Reynolds number of Re=3.17×10⁴. Therefore, $(P_{s,red} - P_s)$ always has a positive value as in Fig. 11(a). Its maximum value all over the pitch and yaw angles is about 14.5 percents of
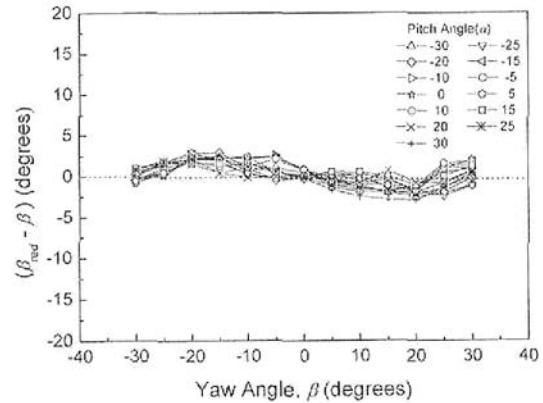

(a) Re=6.60×10³

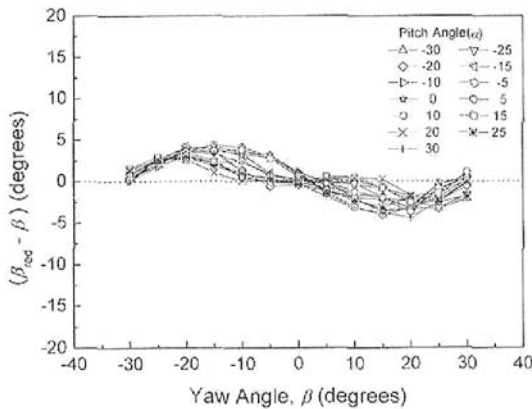(b) Re=1.30×10⁴

Fig. 10 $(\beta_{red} - \beta)$ obtained with calibration coefficients at Re=3.17×10⁴

(a) Re=6.60×10³

(b) Re=1.30×10⁴

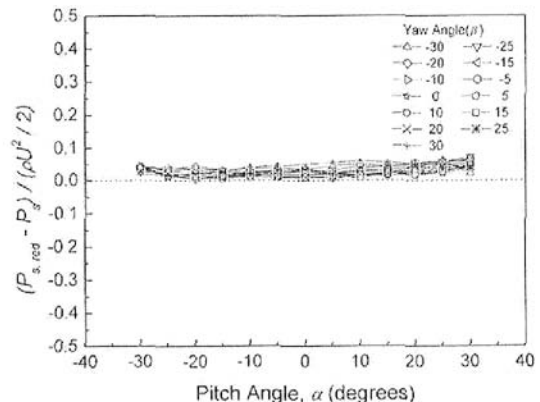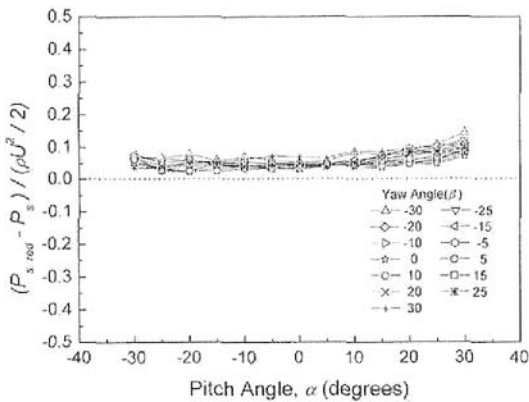**Fig. 11** $(P_{s,red} - P_s)/(\rho U_\infty^2/2)$ obtained with calibration coefficients at Re=3.17×10⁴

$\rho U_\infty^2/2$. Due to the presence of the probe stem, $(P_{s,red}-P_s)$ does not show a perfect symmetric distribution with respect to the line of $\alpha=0$ degree. However, it has a relatively uniform distribution compared with those of $(\alpha_{red}-\alpha)$ in Fig. 9(a) and $(\beta_{red}-\beta)$ in Fig. 10(a). As the Reynolds number increases, $(P_{s,red}-P_s)$ tends to decrease. At Re$=1.30\times10^4$, $(P_{s,red}-P_s)$ has a more uniform distribution than that at Re$=6.60\times10^3$, and its maximum value is reduced to about 7.2 percents of $\rho U_\infty^2/2$.

The reduced total-pressure difference normalized by $\rho U_\infty^2/2$, $(P_{t,red}-P_t)/(\rho U_\infty^2/2)$, is reported in Fig. 12. Figure 8(d) shows that the value of C_{tp} at Re$=6.60\times10^3$ is lower than that at the reference Reynolds number of Re$=3.17\times10^4$, except in the region around the point of α and $\beta=0$ degree. Therefore, most of $(P_{t,red}-P_t)$ has a negative value in contrast with the positive value of $(P_{s,red}-P_s)$. At Re$=6.60\times10^3$, $(P_{t,red}-P_t)$ varies widely from about -21 percents of $\rho U_\infty^2/2$ to 2 percents. When $|\alpha|<15$ degrees, the values of $(P_{t,red}-P_t)$ are usually lower by about 10 percents of $\rho U_\infty^2/2$. On the other hand, its values in the region of $|\alpha|>20$ degrees are higher than about 15 percents of $\rho U_\infty^2/2$ when $|\beta|>20$ degrees. This is attributed mainly to the significant Reynolds-number effects on C_{tp} at the corners in Fig. 8(d). Due to this remarkable Reynolds-number effect, care should be taken in the measurement of the total pressure for flows with these large flow angles. In general, $(P_{t,red}-P_t)$ in

Fig. 12(a) suffers more considerable changes with the variations of the pitch and yaw angles than $(P_{s,red}-P_s)$ in Fig. 11(a), which is resulted from larger variation of C_{tp} with the Reynolds number and its steeper gradient in comparison with those of C_{sp}. As mentioned earlier, the reduced pitch and yaw angles have an influence on the static- and total-pressure determinations. The steeper gradient of C_{tp} than that of C_{sp} may deliver more influences of α_{red} and β_{red} on $P_{t,red}$ than on $P_{s,red}$. It is noted from Figs. 11(a) and 12(a) that the absolute value of $(P_{s,red}-P_s)/(\rho U_\infty^2/2)$ is higher than that of $(P_{t,red}-P_t)/(\rho U_\infty^2/2)$, when $|\alpha|$ and $|\beta|<15$ degrees. This is due to the fact that C_{sp} is more sensitive to the Reynolds number than C_{tp} in this area. As the Reynolds number increases, the absolute value of $(P_{t,red}-P_t)$ tends to decrease, but its general trend remains unchanged as can be seen in Fig. 12(b). At Re$=1.30\times10^4$, the lower bound of $(P_{t,red}-P_t)$ reaches about -18 percents of $\rho U_\infty^2/2$.

The reduced velocity magnitude, Q_{red}/U_∞, is presented in Fig. 13. Q_{red} is evaluated based on Eq. (6). Thus, the reduced velocity magnitude is dependent upon the values of $P_{s,red}$ and $P_{t,red}$. As shown in Figs. 11 and 12, most of $P_{s,red}$ is higher than corresponding P_s, but most of $P_{t,red}$ is lower than corresponding P_t. Therefore, most of $(P_{t,red}-P_{s,red})$ should be lower than (P_t-P_s), which is why most of Q_{red} is lower than the measured velocity magnitude, Q, or U_∞, as can
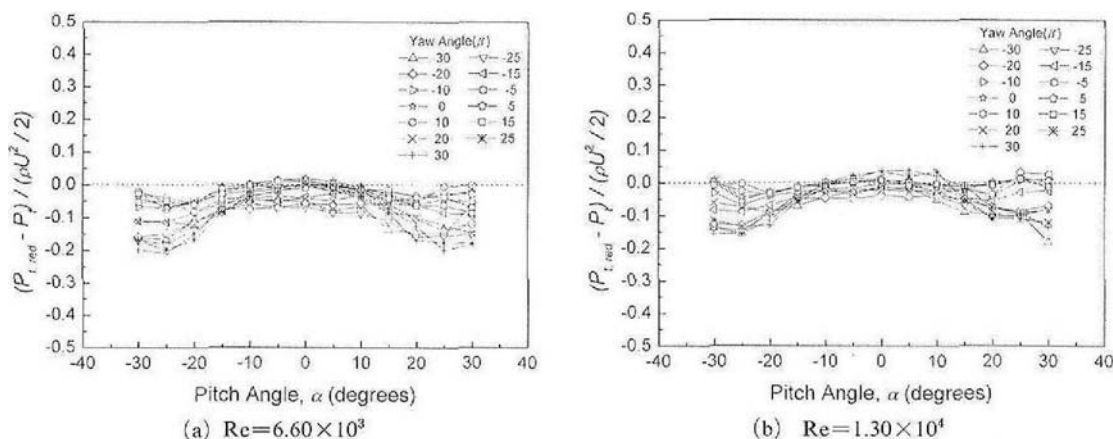

(a) Re$=6.60\times10^3$

(b) Re$=1.30\times10^4$

Fig. 12 $(P_{t,red}-P_t)/(\rho U_\infty^2/2)$ obtained with calibration coefficients at Re$=3.17\times10^4$

be seen in Fig. 13. The general qualitative trend of Q_{red}/U_∞ is very similar to that of $(P_{t,red}-P_t)/(\rho U_\infty^2/2)$, because $(P_{s,red}-P_s)/(\rho U_\infty^2/2)$ has a nearly uniform distribution. The deviation of Q_{red}/U_∞ from unity is relatively small when $|\alpha|$ <15 degrees, but is fairly large when $|\alpha|>20$

degrees. At Re=6.60×10^3 (Fig. 13(a)), the upper and lower bounds of Q_{red}/U_∞ are about 1.01 and 0.88, respectively. At Re=1.30×10^4 (Fig. 13(b)), the lower bound of Q_{red}/U_∞ increases to 0.91.

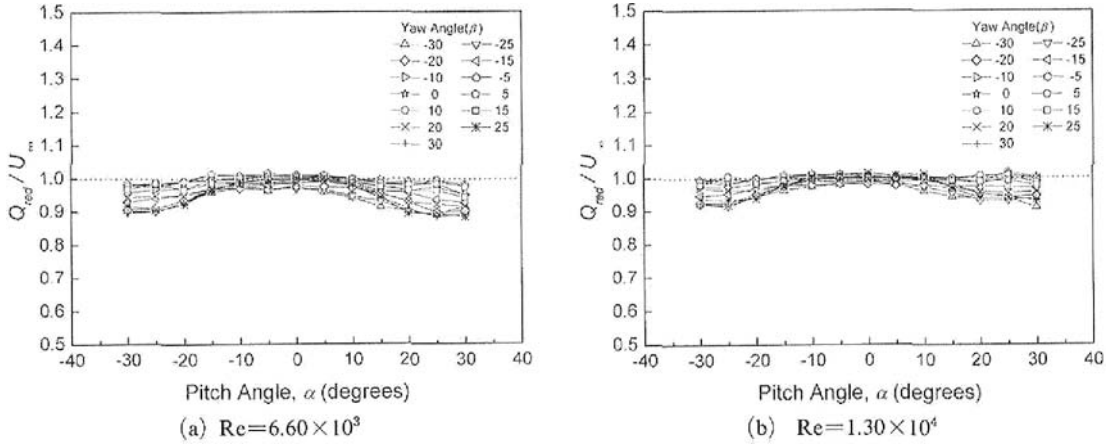In Table 1 and Table 2, the root-mean-square

(a) Re=6.60×10^3 (b) Re=1.30×10^4

Fig. 13 Q_{red}/U_∞ obtained with calibration data at Re=3.17×10^4

Table 1 Upper and lower bounds of the differences between the reduced and measured values obtained with calibration coefficients at Re=3.17×10^4

	$(\alpha_{red}-\alpha)$ (degrees)		$(\beta_{red}-\beta)$ (degrees)		$\dfrac{(P_{s,red}-P_s)}{\rho U_\infty^2/2}$		$\dfrac{(P_{t,red}-P_t)}{\rho U_\infty^2/2}$		$\dfrac{(Q_{red}-U_\infty)}{U_\infty}$	
	Max.	Min.	Max.	Min.	Max.	Min.	Max.	Min.	Max.	Min.
Re=6.60×10^3	4.94	−4.28	4.37	−4.41	0.145	0.022	0.019	−0.209	0.014	−0.118
Re=1.30×10^4	3.20	−2.30	2.90	−2.94	0.072	0.004	0.039	−0.180	0.014	−0.089
Re=1.90×10^4	2.31	−1.75	2.37	−1.94	0.045	−0.007	0.067	−0.168	0.037	−0.077
Re=2.44×10^3	2.23	−1.81	2.34	−1.49	0.042	−0.012	0.051	−0.138	0.028	−0.067
Re=2.87×10^4	2.26	−1.02	2.22	−1.15	0.032	−0.014	0.048	−0.074	0.025	−0.028
Re=3.17×10^4 (Repeatability)	1.95	−1.37	0.77	−1.03	0.008	−0.019	0.026	−0.041	0.016	−0.015

Table 2 Root-mean-square data of the differences between the reduced and measured values obtained with calibration coefficients at Re=3.17×10^4

	$(\alpha_{red}-\alpha)$ (degrees)	$(\beta_{red}-\beta)$ (degrees)	$\dfrac{(P_{s,red}-P_s)}{\rho U_\infty^2/2}$	$\dfrac{(P_{t,red}-P_t)}{\rho U_\infty^2/2}$	$\dfrac{(Q_{red}-U_\infty)}{U_\infty}$
Re=6.60×10^3	2.09	2.20	0.061	0.083	0.050
Re=1.30×10^4	1.37	1.42	0.032	0.059	0.032
Re=1.90×10^4	1.00	1.02	0.018	0.044	0.021
Re=2.44×10^4	0.83	0.79	0.015	0.029	0.015
Re=2.87×10^4	0.66	0.59	0.009	0.016	0.009
Re=3.17×10^4 (Repeatability)	0.55	0.29	0.005	0.010	0.005

values as well as the upper and lower bounds of $(\alpha_{red}-\alpha)$, $(\beta_{red}-\beta)$, $(P_{s,red}-P_s)/(\rho U_\infty^2/2)$, $(P_{t,red}-P_t)/(\rho U_\infty^2/2)$ and $(Q_{red}-U_\infty)/U_\infty$ are reported as a function of the Reynolds number. These values at each Reynolds number are taken among 169 reduced data at the pitch and yaw angles in range, -30 degrees $\leq \alpha$ and $\beta \leq 30$ degrees. In particular, the data listed in the last row in Table 1 and Table 2 are obtained through additional repeatability tests at Re$=3.17\times10^4$ for 144 (12$\times$12) pitch- and yaw-angle pairs which are randomly chosen within each grid in Fig. 4 (d). Thus, they represent errors arising only from the present instrumentation and non-nulling data reduction. If the reduced values in Table 1 and Table 2 at each Reynolds number are compared with the corresponding ones from the repeatability tests, their net changes solely out of the Reynolds-number effect can be estimated. It should be noted that each upper (or lower) bound of the reduced values at a given Reynolds number in Table 1 is not always found at the same pitch- and yaw-angle pair, because each reduced one has its own trend as can be seen in Figs. 9~13.

Table 1 shows that the absolute values of $(\alpha_{red}-\alpha)$ and $(\beta_{red}-\beta)$ are within 5 degrees even at Re$=6.60\times10^3$ and tend to decrease as the Reynolds number decreases. Finally at Re$=2.87\times10^4$, they are less than about 2.3 degrees. The upper bound of $(P_{s,red}-P_s)$ decreases from 14.5 percents of $(\rho U_\infty^2/2)$ at Re$=6.60\times10^3$ to 3.2 percents at Re$=2.87\times10^4$, meanwhile the lower one is changed from 2.2 percents of $(\rho U_\infty^2/2)$ at Re$=6.60\times10^3$ to -1.4 percents at Re$=2.87\times 10^4$. On the contrary, the upper bound of $(P_{t,red}-P_t)$ increases from 1.9 percents of $(\rho U_\infty^2/2)$ at Re$=6.60\times10^3$ to 4.8 percents at Re$=2.87\times10^4$, while the lower one of $(P_{t,red}-P_t)$ varies from -20.9 percents of $(\rho U_\infty^2/2)$ at Re$=6.60\times10^3$ to -7.4 percents at Re$=2.87\times10^4$. The upper and lower bounds of $(Q_{red}\times U_\infty)$ varies from 1.4 and -11.8 percents of U_∞ at Re$=6.60\times10^3$ to 2.5 and -2.8 percents at Re$=2.87\times10^4$, respectively. Table 2 shows that each root-mean-square value gradually decreases as the Reynolds number increases. It is interesting that the root-mean-

square value of $(\alpha_{red}-\alpha)$ at each Reynolds number is approximately the same as that of $(\beta_{red}-\beta)$. As expected, the root-mean-square values from the repeatability tests in Table 2 are always less than those at Re$=2.87\times10^4$.

In the present non-nulling reduction procedure, the calibration coefficients at the highest Reynolds number are employed as input reference calibration data. For a comparison purpose, we employed the calibration coefficients at the lowest Reynolds number (Re$=6.60\times10^3$) as input reference calibration data. This shows totally reversed tendencies : The positive values of $(\alpha_{red}-\alpha)$ and $(\beta_{red}-\beta)$ turn to be negative, and vice versa. Most of $(P_{s,red}-P_s)$ becomes negative meanwhile most of $(P_{t,red}-P_t)$ and $(Q_{red}-U_\infty)$ have positive values.

In order to account for the Reynolds-number effect perfectly, calibrations should be carried out over the wide range of the Reynolds number, and then the reference calibration data could be selected among them, depending on the local Reynolds number at each measurement location. However, this is unrealistic, because each local velocity magnitude remains unknown. In an actual measurement, instead, it would be more practical to specify errors associated with the Reynolds-number effect. Therefore, the data listed in Table 1 and 2 will be very useful in the estimation of the Reynolds-number effect.

4. Conclusions

The effects of the Reynolds number on the five-hole probe calibration in a non-nulling mode have been investigated for the representative Reynolds numbers in turbomachinery. For a typical cone-type five-hole probe, the pitch and yaw angles are changed from -35 degrees to 35 degrees with an angle interval of 5 degrees at six probe Reynolds numbers in range between 6.60×10^3 and 3.17×10^4. The major effects of the Reynolds number on the calibration coefficients are summarized as follows :

(1) Not only each calibration coefficient itself but also its Reynolds number dependency is

affected significantly by both pitch and yaw angles. In this study, the combined effects of the pitch and yaw angles on the calibration coefficients are discussed in detail.

(2) When the absolute values of the pitch and yaw angles are smaller than 20 degrees, there is a noticeable Reynolds-number effect on the pitch- and yaw-angle coefficients, and their absolute values in this region tend to increase with increasing the Reynolds number.

(3) The static-pressure coefficient is found sensitive to the Reynolds number nearly all over the pitch- and yaw-angle range. With increasing the Reynolds number, most of the static-pressure coefficient tends to decrease.

(4) There exists a remarkable Reynolds-number effect on the total-pressure coefficient when the absolute values of the pitch and yaw angles are larger than 20 degrees, which seems to be the most noticeable Reynolds-number effect among the four calibration coefficients. With increasing the Reynolds number, most of the total-pressure coefficient has a tendency to increase.

In turbomachinery applications, flows near machine surfaces and in wake regions, where most of aerodynamic losses are generated, may have a lower local velocity than the free-stream velocity. Noting this fact, actual reduced values of the flow angles, pressures and velocity magnitude at each Reynolds number are obtained through a typical non-nulling reduction procedure, employing the calibration coefficients at the highest Reynolds number $(Re=3.17\times10^4)$ as input reference calibration data. The Reynolds-number effects on the reduced values are summarized as follows:

(5) The general tendency of each reduced value is related closely to the variation of the corresponding calibration coefficient with the Reynolds number, and each reduced one has its own unique trend. As the Reynolds number approaches the reference one, the Reynolds-number effects tend to diminish.

(6) The trend of the reduced pitch-angle difference, $(\alpha_{red}-\alpha)$, with α is nearly the same as that of the reduced yaw-angle difference, $(\beta_{red}-\beta)$, with β. Each of them has a positive value at

the pitch and yaw angles where the corresponding calibration coefficient is higher than that at the reference Reynolds number, and vice versa.

(7) Regardless of the Reynolds number, most of the reduced static pressure, $P_{s,red}$, has a higher value than the measured one, P_s, while most of the reduced total pressure, $P_{t,red}$, has a lower value than the measured one, P_t. In general, $(P_{s,red}-P_s)$ has a relatively uniform distribution, but $(P_{t,red}-P_t)$ suffers more considerable changes with the variation of the pitch and yaw angles. Particularly when the absolute values of the pitch and yaw angles are larger than 20 degrees, the reduced total pressure suffers the most considerable deviation from the measured one among all the reduced values.

(8) Regardless of the Reynolds number, most of the reduced velocity magnitude, Q_{red}, is lower than the measured velocity magnitude, and its general trend is similar to that of $(P_{t,red}-P_t)$.

(9) In this study, the root-mean-square data as well as the upper and lower bounds of each reduced value are reported as a function of the Reynolds number, in addition to repeatability test data at the reference Reynolds number. These data would be very useful in the estimation of the Reynolds-number effects on the non-nulling calibration.

References

Abernethy, R. B., Benedict, R. P. and Dowdell, R. B., 1985, "ASME Measurement Uncertainty," *ASME Journal of Fluids Engineering*, Vol. 107, pp. 161~164.

Anderson, J. D., Jr., 1990, *Modern Compressible Flow with Historical Perspective*, Series in Aeronautical and Aerospace Engineering, Mc-Graw-Hill, p. 6.

Coldrick, S., Ivey, P. and Wells, R., 2002, "Considerations for Using 3D Pneumatic Probes in High Speed Axial Compressor," ASME Paper No. GT-2002-30045.

Dominy, R. G. and Hodson, H. P., 1993, "An Investigation of Factors Influencing the Calibration of Five-Hole Probes for Three-Dimensional Flow Measurement," *ASME Journal of*

Turbomachinery, Vol. 115, pp. 513~519.

Hoffmann, G. D., Rabe, D. C. and Poti, N. D., 1980, "Flow Direction Probes from a Theoretical and Experimental Point of View," *Journal of Physics E-Scientific Instruments*, Vol. 13, pp. 751~760.

Koschel, W. and Pretzsch, P., 1988, "Development and Investigation of Cone-Type Five-Hole Probes for Small Gas Turbine," *Proceedings Of 9th Symposium on Measuring Techniques in Transonic and Supersonic Flows in Cascade and Turbomachines*, Oxford, United Kingdom.

Lee, S. W., Lee, J. S. and Ro, S. T., 1994, "Experimental Study on the Flow Characteristics of Streamwise Inclined Jets in Crossflow on Flat Plate," *ASME Journal of Turbomachinery*, Vol. 116, pp. 97~105.

Lee, S. W., Kim, Y. B. and Lee, J. S., 1997, "Flow Characteristics and Aerodynamic Losses of Film-Cooling Jets with Compound Angle Orientations," *ASME Journal of Turbomachinery*, Vol. 119, pp. 310~319.

Lee, S. W., Park, S. W. and Lee, J. S., 2001a, "Flow Characteristics Inside Circular Injection Holes Normally Oriented to a Crossflow: Part I — Flow Visualizations and Flow Data in the Symmetry Plane," *ASME Journal of Turbomachinery*, Vol. 123, pp. 266~273.

Lee, S. W., Joo, S. K. and Lee, J. S., 2001b,

"Flow Characteristics Inside Circular Injection Holes Normally Oriented to a Crossflow: Part II — Three-Dimensional Flow Data and Aerodynamic Loss," *ASME Journal of Turbomachinery*, Vol. 123, pp. 274~280.

Lee, S. W. and Yoon, T. J., 1999, "An Investigation of Wall-Proximity Effect Using a Typical Large-Scale Five-Hole Probe," *KSME International Journal*, Vol. 13, pp. 273~285.

Ligrani, P. M., Singer, B. A. and Baun, L. R., 1989, "Spatial Resolution and Downwash Velocity Corrections for Multiple-Hole Pressure Probe in Complex Flow," *Experiments in Fluids*, Vol. 7, pp. 424~426.

Prenter, P. M., 1975, *Splines and Variational Methods*, Wiley-Intersciences.

Sitaram, N., Lakshminarayana, B. and Ravindranath, A., 1981, "Conventional Probes for the Relative Flow Measurement in a Turbomachinery Rotor Blade Passage," *ASME Journal of Turbomachinery*, Vol. 103, pp. 406~414.

Smith, A. L. and Adcock, J. B., 1986, "Effect of Reynolds Number and Mach Number on Flow Angularity Probe Sensitivity," NASA TM-87750.

Treaster, A. L. and Yocum, A. M., 1979, "The Calibration and Application of Five-Hole Probes," *ISA Transactions*, Vol. 18, pp. 23~34.